J|A|C|S
ARTICLES
Published on Web 03/22/2002

CdS Nanoparticles Modified to Chalcogen Sites: New Supramolecular Complexes, Butterfly Bridging, and Related Optical Effects

Tong Ni,[†] Dattatri K. Nagesha,[†] Juvencio Robles,[‡] Nicholas F. Materer,[†] Stefan Müssig,[†,§] and Nicholas A. Kotov*[,†]

Contribution from the Chemistry Department, Oklahoma State University, Stillwater, Oklahoma 74078, and Facultad de Quimica, University of Guanajuato, Noria Alta s/n, Guanajuato, GTO, 36050, Mexico

Received September 24, 2001. Revised Manuscript Received February 7, 2002

Abstract: All present approaches to surface modification of nanoparticles (NPs) with organic ligands exploit metal (cadmium) sites as anchor points. To obtain efficient interaction of NP surface with p-orbitals of organic chromophores, we utilize the chalcogen (sulfur) sites on the NP surface. These sites present several advantages stemming from a stronger interaction of their atomic orbitals with both modifier and NP core. The chalcogen modification of CdS was achieved by using a mixed ligand (2,2′-bipyridyl-*N*,*N*′)(malonato-*O*,*O*′)-copper(II) monohydrate complex. The weak monodentate ligands (water) are replaced by a copper−sulfur bond during the modification reaction. The structure of the product was investigated by optical spectroscopy, electron spin resonance, and nuclear magnetic resonance. The modified NP can be described as a few tens (<40) of (2,2′-bipyridyl-*N*,*N*′)(malonato-*O*,*O*′)-copper units attached to the CdS core. Steady-state and time-resolved luminescence measurements, molecular orbital calculations, and UPS data indicate that delocalized surface states enveloping the surface chalcogen atoms of NP, transition metal, and p-orbitals of the bipyridine ligand are present in the synthesized species. The delocalized states are made possible due to the bridging of p-levels of sulfur and π-orbitals of bipyridine by butterfly d-orbitals of the transition metal atom placed between them. Chalcogen-modified NP can be considered as a new member of the family of supramolecular compounds based on transition metal complexes. Both NP and metal complex parts of the prepared supramolecules are very versatile structural units, and new molecular constructs of similar design, in which quantum effects of NPs are combined with optical properties of transition metal complexes, can be obtained with different NPs and metal complexes.

Introduction

II-VI semiconductor nanoparticles (NPs), such as cadmium chalcogenides, represent a new type of chromophores for which adsorption and emission bands are controlled by the diameter of the particle.[1] Surface-modified NPs are some of the most intriguing objects for future studies. Surface modification was shown to optimize the intrinsic optical properties of nanomaterials producing highly luminescent colloids[2] with a variety of applications, and their modification also serves as a convenient tool aiding in the investigation of complex electronic processes in NPs.[3,4] At the same time, surface ligands with chemical specificity can introduce a higher level of NP structural organization and new chemical/optical properties related to their collective behavior. In many studies on the surface modification of II-VI semiconductor NPs with different organic ligands, their pairing with optically active compounds such as dyes, aromatic hydrocarbons, etc., was aimed at finding the effects from the charge carrier exchange between the electronic levels of a NP core and a modifier.[5] There are direct UV−vis spectroscopy pieces of evidence about the existence of such effects in very small $Cd_{32}S_{14}$ clusters that have been obtained.[6,7] There is also other evidence of NP-NP and NP-modifier carrier exchange as conductivity changes in NP-polymer composites when interparticle bridges replace partially the stabilizer layer

* To whom correspondence should be addressed. E-mail: Kotov@okstate.edu.
[†] Oklahoma State University.
[‡] University of Guanajuato.
[§] Permanent address: Chemistry Department, University of Hamburg, Martin-Luther-King-Platz 6, 20146 Hamburg, Germany.

(1) Weller, H. *Curr. Opin. Colloid Interface Sci.* **1998**, *3*, 194−199. Weller, H.; Eychmueller, A. *Adv. Photochem.* **1995**, *20*, 165−216. Weller, H. *Adv. Mater.* (*Weinheim, Ger.*) **1993**, *5*, 88−95. Weller, H. *Angew. Chem.* **1993**, *105*, 43−55. Alivisatos, A. P. *Science* (*Washington, D.C.*) **2000**, *289*, 736−737. Alivisatos, P. *Pure Appl. Chem.* **2000**, *72*, 3−9. Alivisatos, A. P. *Endeavour* **1997**, *21*, 56−60. Alivisatos, A. P. *J. Phys. Chem.* **1996**, *100*, 13226−13239. Alivisatos, A. P. *MRS Bull.* **1995**, *20*, 23−32. Bawendi, M. G. *Solid State Commun.* **1998**, *107*, 709. Bawendi, M. G. *Nato Asi Ser., Ser. B* **1995**, *340*, 339−356.
(2) Dabbousi, B. O.; Rodriguez-Viejo, J.; Mikulec, F. V.; Heine, J. R.; Mattoussi, H.; Ober, R.; Jensen, K. F.; Bawendi, M. G. *J. Phys. Chem. B* **1997**, *101*, 9463−9475. Peng, X. G.; Schlamp, M. C.; Kadavanich, A. V.; Alivisatos, A. P. *J. Am. Chem. Soc.* **1997**, *119*, 7019−7029. Hines, M. A.; Guyot-Sionnest, P. *J. Phys. Chem.* **1996**, *100*, 468.
(3) Klimov, V. I.; Mikhailovski, A. A.; McBranch, D. W.; Leatherdale, C. A.; Bawendi, M. G. *Phys. Rev. B.* **2000**, *61*, R13349.
(4) Guyot-Sionnest, P.; Shim, M.; Matranga, C.; Hines, M. *Phys. Rev. B* **1999**, *60*, 2181.

10.1021/ja017149a CCC: $22.00

and stimulate such processes via conjugation through aromatic heterocycles[8−11] or aromatic thiols.[10,12]

All current strategies of II-VI semiconductor NP functionalization are based either on the exchange of a stabilizer bound to the metal sites on the NP's surface or on the chemical modification of its terminal group. There is a substantial energy mismatch between the surface Cd ions and the conduction band of the semiconductor NPs, which creates an energetic hurdle for the effective interaction between the carrier levels.[13] This barrier is much lower for corresponding S and Se sites because, unlike metal sites, the energy states of surface S or Se atoms are partially mixed with the valence band of CdS or CdSe, respectively.[13] This low barrier makes them suitable for the preparation of conjugated electronic systems. These considerations prompted us to investigate the chalcogen atoms as possible sites for surface modification of NP. We report here on a new synthetic approach to utilize S sites of CdS for surface modification and demonstrate the formation of novel supramolecular structures made of NP and transition metal complexes. Efficient bridging of the p-orbitals of sulfur on the surface of NP and the π-system of aromatic ligand was made possible by butterfly d-orbitals of the transition metal sandwiched between them. This bonding results in the formation of new delocalized electronic states embracing surface atoms of NP, metal atom, and ligands of the complex. Such states result in novel features in the photophysics of surface modified NPs, for instance, the excitation energy transfer from the modifier to the surface states and in the appearance of new luminescence band(s). The delocalized surface states can profoundly influence the electronic processes at the NP surface such as carrier trapping, charge recombination of different types, photoinduced absorption, and charge injection into the NPs. Such systems would be of great interest for many applications of NPs including molecular electronics, catalysis, and NP lasing actively discussed in the scientific literature nowadays,[3,14,15] albeit anticipated problems related to their photochemical stability will still need to be resolved. The fact that both NP and metal complexes are versatile chromophores, just like organic aromatic compounds, and their permutations can produce a large new class of supramolecular compounds, for which the quantum effects of NPs are combined with optical properties of transition metal complexes, is also important.[16]

Experimental Section

Chemicals. $Cd(ClO_4)_2 \cdot 4H_2O$ (Aldrich), thioacetamide (Aldrich), $CuCl_2 \cdot H_2O$ (Aldrich), malonic acid (Aldrich), ethylene glycol (Aldrich), Na_2S (Fluka), 2,2′-bipyridine (Sigma), Rhodamine B (Fluka), dimethylformamide (EM Sciences), sodium citrate (EM Science), NaOH (EM Science), and acetone (Aldrich, Fisher) were of A.C.S. reagent grade and were used without further purification. Water (18 MOhm) obtained from the Barnstead E-pure system was used in all preparations.

Procedures. Synthesis. CdS quantum dots were synthesized by microwave heating of aqueous solution of cadmium perchlorate with thioacetamide as a source of sulfide ions. Next 0.025 g of sodium citrate (stabilizer) was dissolved in 45 mL of deionized water. After the pH was adjusted to 9.2, 2 mL of 10^{-2} M $Cd(ClO_4)_2$ and 2.5 mL of 8×10^{-3} M thioacetamide were added, and the pH was readjusted again to 9.2. The mixture of precursors was heated in a conventional Sharp microwave oven at 1000 W continuously for 60 s and then stored in the dark at room temperature for ripping for 2−3 days. According to this procedure, one can typically obtain particles of an average diameter of 44 Å. Different sizes of CdS NPs were obtained by increasing the concentration of Cd^{2+} to 2×10^{-2}, 4×10^{-2}, and 6×10^{-2} M, which gives the average particle size of 35, 30, and 26 Å. The diameter of the particles was evaluated on the basis of the UV−vis spectra by using the correlation between absorption onset and particle diameter[17] and transmission electron microscopy imaging.

Synthesis of (2,2′-bipyridyl-*N*,*N*′)(malonato-*O*,*O*′)-copper(II) monohydrate (CuBM) was synthesized according to ref 18. Briefly, 177 mg of $CuCO_3 \cdot Cu(OH)_2$ (0.79 mmol), 43 mg of Na(OH) (0.9 mmol), 83 mg of malonic acid (0.79 mmol), and 124 mg of 2,2′-bipyridine (0.79 mmol) were combined in 40 mL of distilled water and refluxed for 3 h. The solution was concentrated in a rotary evaporator until small crystals appeared. The reaction vessel was then cooled, and the solid was allowed to precipitate. The blue crystalline product was washed three times in acetone followed by drying in a vacuum. CuBM was obtained with the yield of 48.3%.

Theoretical and Computational Methodology. Theoretical calculations were performed to gain insight on the details of the excitation transfer between the core NP and the CuBM surface modifier. Because of the thousands of atoms occurring at the NP of the experimentally studied sizes, the computational cost is prohibitive even with state-of-the-art hardware and software. Therefore, our previous successfully employed cluster model[19] is used to simulate the NP-modifier system.

Once the cube model cluster was set for the NP-modifier system, a theoretical method was chosen to obtain the optimized geometry, wave function, and derived properties. We initially obtained a semiempirical[20,21] PM3 optimized geometry. The obtained geometry was tested

(5) Kuno, M.; Lee, J. K.; Dabbousi, B. O.; Mikulec, F. V.; Bawendi, M. G. *J. Chem. Phys.* **1997**, *106*, 9869−9882. Majetich, S. A.; Carter, A. C. *J. Phys. Chem.* **1993**, *97*, 8727−8731. Veinot, J. G. C.; Ginzburg, M.; Pietro, W. J. *Chem. Mater.* **1997**, *9*, 2117−2122. Veinot, J. G. C.; Galloro, J.; Pugliese, L.; Bell, V.; Pestrin, R.; Pietro, W. J. *Can. J. Chem.* **1998**, *76*, 1530−1539. Kumar, A.; Kumar, S. *J. Photochem. Photobiol., A* **1994**, *83*, 251−256. Tata, M.; Banerjee, S.; John, V. T.; Waguespack, Y.; Mcpherson, G. L. *Colloids Surf., A* **1997**, *127*, 39−46. Deng, H. H.; Li, M.; Zhang, Y.; Lu, Z. H.; Fu, D. G. *Chem. Lett.* **1997**, 483−484. Thomas, K. G.; Kamat, P. V. *J. Am. Chem. Soc.* **2000**, *122*, 2655−2656. Noglik, H.; Pietro, W. J. *Chem. Mater.* **1994**, *6*, 1593−1595. Farah, A. A.; Pietro, W. J. *Polym. Bull.* **1999**, *43*, 135−142. Veinot, J. G. C.; Ginzburg, M.; Pietro, W. J. *Chem. Mater.* **1997**, *9*, 2117−2122. Noglik, H.; Pietro, W. J. *Chem. Mater.* **1995**, *7*, 1333−1336. Chandler, R. R.; Coffer, J. L. *J. Phys. Chem.* **1991**, *95*, 4−6. Lahav, M.; Shipway, A. N.; Willner, I.; Nielsen, M. B.; Stoddart, J. F. *J. Electroanal. Chem.* **2000**, *482*, 217−221. Mahtab, R.; Harden, H. H.; Murphy, C. J. *J. Am. Chem. Soc.* **2000**, *122*, 14−17. Mahtab, R.; Rogers, J. P.; Murphy, C. J. *J. Am. Chem. Soc.* **1995**, *117*, 9099−9100. Lahav, M.; Gabriel, T.; Shipway, A. N.; Willner, I. *J. Am. Chem. Soc.* **1999**, *121*, 258−259. Nabok, A. V.; Ray, A. K.; Hassan, A. K. *J. Appl. Phys.* **2000**, *88*, 1333−1338. Liu, J.; Mendoza, S.; Roman, E.; Lynn, M. J.; Xu, R.; Kaifer, A. E. *J. Am. Chem. Soc.* **1999**, *121*, 4304−4305. Konovalova, T. A.; Kispert, L. D.; Konovalov, V. V. *J. Phys. Chem. B* **1999**, *103*, 4672−4677. Boal, A. K.; Rotello, V. M. *J. Am. Chem. Soc.* **1999**, *121*, 4914−4915. Sooklal, K.; Hanus, L. H.; Ploehn, H. J.; Murphy, C. J. *Adv. Mater.* (*Weinheim, Ger.*) **1998**, *10*, 1083−1087.

(6) Vossmeyer, T.; Reck, G.; Schulz, B.; Katsikas, L.; Weller, H. *J. Am. Chem. Soc.* **1995**, *117*, 12881−12882.

(7) Doellefeld, H.; Weller, H.; Eychmueller, A. *Nano Lett.* **2001**, *1*, 267−269.

(8) Winiarz, J. G.; Zhang, L.; Lal, M.; Friend, C. S.; Prasad, P. N. *J. Am. Chem. Soc.* **1999**, *121*, 5287−5295.

(9) Veinot, J. G. C.; Farah, A. A.; Galloro, J.; Zobi, F.; Bell, V.; Pietro, W. J. *Polyhedron* **2000**, *19*, 331−341.

(10) Majetich, S. A.; Carter, A. C.; McCullogh, R. D. *Mater. Res. Soc. Symp. Proc.* **1993**, *286*, 87−92.

(11) Greenham, N. C.; Peng, X.; Alivisatos, A. P. *Synth. Met.* **1997**, *84*, 545−546.

(12) Bertoncello, R.; Bettinelli, M.; Casarin, M.; Maccato, C.; Pandolfo, L.; Vittadini, A. *Inorg. Chem.* **1997**, *36*, 4707−4716.

(13) Bawendi, M. G.; Carroll, P. J.; Wilson, W. L.; Brus, L. E. *J. Chem. Phys.* **1992**, *96*, 946−954.

(14) Klein, D. L.; Roth, R.; Lim, A. K. L.; Alivisatos, A. P.; McEuen, P. L. *Nature* **1997**, *389*, 699−701.

(15) Torres-Martinez, C. L.; Nguyen, L.; Kho, R.; Bae, W.; Bozhilov, K.; Klimov, V.; Mehra, R. K. *Nanotechnology* **1999**, *10*, 340−354.

(16) The publications on the surface modification of CdSe and In2S3 with different metal complexes including ruthenium bipyridines are being prepared.

(17) Vossmeyer, T.; Katsikas, L.; Giersig, M.; Popovic, I. G.; Diesner, K.; Chemseddine, A.; Eychmueller, A.; Weller, H. *J. Phys. Chem.* **1994**, *98*, 8, 7665−7673.

(18) Suresh, E.; Bhadbhade, M. M. *Acta Crystallogr.* **1997**, *C53*, 193−195.

(19) Diaz, D.; Robles, J.; Ni, T.; Castillo-Blum, S. E.; Nagesha, D.; Alvarez-Fregoso, O. J.; Kotov, N. A. *J. Phys. Chem. B* **1999**, *103*, 9859−9866.

to correspond to a global potential minimum through analysis of the resulting Hessian frequencies. Keeping this geometry, we thereafter obtained single point energy, wave function, and orbitals at a higher level of theory,[20] performing a density functional calculation[22] with the exchange functional of Becke[23] and the correlation functional of Perdew.[24] The DN(*) numerical basis set, similar in size to the 6-31G(d) Gaussian basis set,[25] was used. Furthermore, post SCF gradient corrections are included on a perturbative manner. Therefore, the achieved level of calculation is p-BP86/DN(*)//PM3.

Instrumentation. UV−Vis. Optical absorption spectra were obtained on a Hewlett−Packard 8453 diode array spectrophotometer using 1 cm quartz cuvettes in air under room temperature. All spectra were measured against air except Rhodamine B, which was measured against ethylene glycol.

Steady-State Emission. Fluorescence spectra were recorded on a Fluorolog 3 from JY-SPEX (ISA) modular spectrofluorimeter operating with a 450 W xenon arc lamp as a light source. Typically, the wavelength increment was set at 1 nm, integration time for each point was 0.4 s, and slit width (expressed as band-pass) was varied between 2 and 10 nm according to the signal intensity. Emission of each batch of samples was first analyzed for different excitation wavelengths to separate excitation-energy-independent peaks and excitation-energy-dependent peaks from Raman and Rayleigh scattering. The excitation wavelength was chosen to minimize the interference of the latter with the luminescence signals. All the conditions were kept constant for sample series. Corrected S signal was used for emission spectral measurements, whereas S/R signal was used to record all excitation spectra, which was subsequently corrected by the instrumental function obtained from the excitation profile of Rhodamine B emission. The optical density in excitation spectra measurements was adjusted to below 0.12 units for all the wavelengths of interest. A quartz Dewar vessel (SPEX) filled with liquid nitrogen was used in the low-temperature studies.

Quantum yields were calculated by comparing individually integrated emission peaks with the integrated 580 nm peak of freshly prepared Rhodamine B solution in ethylene glycol. The excitation wavelength was chosen so that both Rhodamine B and CdS displayed identical optical density (345 nm). All emission peaks were Gaussian fitted with four parameters using SigmaPlot scientific graphic software and integrated by GRAMS/386. The baseline of the Gaussian peaks was subtracted from the value of the integral emission intensity.

Time-Resolved Fluorescence. Time-resolved fluorescence measurements were carried out by using two techniques: time-correlated single photon counting and phase modulation. For both techniques, the liquid dispersion was placed in 1 cm quartz cuvettes and examined under ambient conditions. The dispersions were prepared in the same way as for steady-state luminescence measurements and other experiments. For the single photon counting technique, a tunable picosecond pulsed laser system consisting of a cavity-damped dye laser synchronously pumped by a frequency-doubled mode-locked Nd:YAG laser was used as an excitation source. The emission was registered by a streak camera in front-face registration mode. The output laser pulses from the dye laser had a duration time of less than 5 ps and were frequency doubled into the ultraviolet spectral region by a nonlinear crystal. The luminescence intensity versus time curves were processed in the following way. Because the laser pulse times were much shorter than the luminescence lifetimes of the species, the deconvolution of the excitation pulse was not required. The plateau background intensity observed for very long decay times was subtracted from the overall intensity, and then the decay curve was best-fitted with a single exponent, the lifetime for which is reported. This lifetime represents cumulative representation of the decay rate and is not associated with a specific photophysical process.

Our time-resolved photoluminescence measurements start with a Coherent Antares Nd:YAG laser that emits infrared at a wavelength of 1.064 μm with a pulse repetition rate of 76 MHz, a pulse width of 70 ps, and 20 W power averaged over both the on and the off pulse times. External to the laser cavity, but inside the laser head, a second harmonic generation crystal converts the infrared to green with a wavelength of 532 nm and an average power of 5 W. This green light pumps a Coherent dye laser equipped with a cavity dumper. The output of the dye laser and cavity dumper is red light with a tunable wavelength, an average power of about 100 mW, and a pulse width of about 5 ps. The pulse repetition rate of the cavity dumper can be varied between 38 MHz and 147 kHz. This red light is then frequency doubled into ultraviolet, which is directed to the sample. The sample photoluminescence is focused into a small spectrometer, which directs the light into a Hamamatsu C5680 streak camera with a resolution of 2 ps. Although the excitation pulses have a width of 5 ps, the actual time resolution we obtain depends on the streak camera sweep range. For example, for a sweep range of 150 ps, we can measure a 10 ps fwhm for the diffusely reflected excitation laser light. However, when we use a 4 ns sweep range, we may measure a 50 or 100 ps fwhm for the diffusely reflected light. We measure time-resolved photoluminescence in a photon counting mode, in which each lit up pixel area represents one photon in an exposure time of 33 ms. A typical sample measurement has 20 000 exposures and lasts about 11 min.

Time-resolved photoluminescence measurements were also made on a Tau-3 Fluorolog 3, JY-SPEX (ISA), system, which uses cross-correlation frequency domain measurements of the phase shift and demodulation factors (phase shift and ratio of modulated anisotropy) across a frequency range. The phase modulation method measures the response functions of a fluorescent sample from a sinusoidally modulated by the Pockels cell continuous wave source (450 W Xe lamp). Diluted Ludox dispersion was used as a scattering standard for all measurements. The lifetime of emission is calculated by fitting phase shift versus frequency curve by using the software provided by ISA SPEX for frequencies between 0.1 and 100 MHz. Typically, virtually perfect curve fits were obtained for four exponential decay models. In the analysis of the results, only the dominant component responsible for >50% of the luminescence was considered.

Nuclear Magnetic Resonance Spectroscopy (NMR). ^{1}H NMR spectra were recorded at room temperature on an Inova 400 instrument from Varian operating at ^{1}H frequency of 399.96 MHz with ID5 or ID-PFG probe. Water suppression with zero spinning was used in all measurements. The spectra were averaged over 256−2048 scans depending on the signal intensity and the signal-to-noise ratio. The water resonance peak in D_2O at 4.80 ppm was used as a reference for all spectra, and no internal standard was added. For NMR studies, CdS stabilized by sodium citrate was synthesized in D_2O.

Electron Spin Resonance Spectroscopy (ESR). ESR measurements were performed on a Bruker ER 200D SRC with the center of field set at 3280 G, sweep width 800 G, gain 8×10^4, microwave frequency 9.78 GHz, and microwave attenuation 22. The ESR data were collected from a sample placed in a thin quartz cell designed for ESR in aqueous solutions. All measurements were performed at ambient conditions.

Ultraviolet Photoelectron Spectroscopy (UPS). The surface analytical apparatus consists of a ultrahigh vacuum chamber pumped by a 330-L/s ion pump coupled to a load-lock chamber via long stroke manipulator. Typical base pressure is 1×10^{-5} Pa and raises to 1×10^{-3} Pa during He(I) UPS. The sample is placed at a 45° angle with respect to the front of the energy analyzer to avoid photoelectron contributions from the sample holder. A double-pass cylindrical mirror analyzer with a pass energy of 5 eV is used to measure the photoelectrons. This analyzer accepts all electrons within a cone around

(20) Hehre, W. J.; Radom, L.; Schleyer, P. V. R.; Pople, J. A. *Ab Initio Molecular Orbital Theory*; Wiley: New York, 1986.
(21) Stewart, J. J. P. *J. Comput. Chem.* **1989**, *10*, 209.
(22) Parr, R. G.; Yang, W. *Density Functional Theory of Atoms and Molecules*; Oxford University Press: New York, 1989.
(23) Becke, A. D. *Phys. Rev.* **1988**, *A38*, 3089.
(24) Perdew, J. P. *Phys. Rev.* **1986**, *B33*, 8822.
(25) Spartan version 5.1, Wavefunction, Inc.: Irvine, CA, 1998; ref type, generic.

42° from the sample normal. A He discharge source is differentially pumped using a mechanical pump as the first stage and a turbomolecular pump as the second and final stage. The source pressure was adjusted to optimize the He(I) emission that provides photons with an energy of 21.21 eV. The discharge source is positioned slightly less than perpendicular from the face of the energy analyzer. Thus, the sample is illuminated at glancing incidence. To allow direct comparisons between the various modified surfaces, the binding energies are calculated with respect to the vacuum level.

Transmission Electron Microscopy (TEM). A Phillips CM 300 operating at 200 kV was used for transmission electron microscopy. For preparation of samples for electron microscopy, a drop of NP dispersion was placed onto a carbon-coated aluminum grid (200 mesh). The grid was allowed to dry for 1 min, and then blotted with filter paper to remove excess solution. The dried grids were transferred into a nitrogen-filled container and then to the cell compartment of the TEM microscope, equipped with a Phillips EDAX 9800 analyzer. A number of grids were prepared from each sample to check the reproducibility of the preparative procedure. Bright-field images were taken under conditions of minimum phase contrast. Quantitative EDAX analysis (element detection and analysis by X-rays) of individual particles was carried out with the electron microscope in nanoprobe mode (beam spot size reducible down to 1 nm) using a spot size equal to the average diameter of the particles. The size distribution curves were obtained by analyzing crystal lattice-resolved TEM images. For each curve ~70−80 NPs were counted. The reported diameters were the diameters of the areas of continuous crystallinity approximated by a circle to match the total area of unbroken crystal lattice. Large aggregates with indistinguishable interparticle boundaries were neglected in the total count.

X-ray Photoelectron Spectroscopy. X-ray photoelectron spectra (XPS) were recorded at a take-off angle of 0° using a VG EscaLab 220-IXL system. The K_α X-ray line (eV) of aluminum at a spectrometer pass energy of 1486.92 eV and step resolution of 0.1 eV was used as the source. The authors thank Carmen Serra-Rodríguez, from the University of Vigo, Spain, for generous help with XPS experiments.

Theoretical Calculations and Molecular Modeling. All calculations (semiempirical PM3 and density functional theory) were carried out on a Silicon Graphics Octane Workstation (Dual MIPS RISC R10000, 64-bit, 195 MHz/1MB cache processors, IRIX 6.4 operating system, 256 MB RAM, 4.0 GB disk) and an ORIGIN 2000 series with eight R10000 processors. For all calculations and visualizations, the Gaussian 94[26] and Spartan V5.1 software packages were employed.[25]

Results

Atoms of metals have been widely used to anchor organic moieties to the surface of NPs. Chemically, this is the most straightforward method of surface modification because there is a wide variety of readily available organic compounds acting as Lewis bases, which can react with electron-deficient atoms of cadmium and other metals constituting the surface of NPs. By the same token, surface chalcogen atoms can serve as anchor points for compounds acting as Lewis acids. However, finding a suitable Lewis acid/base pair for the modification of chalcogen atoms is more difficult than for the electron-deficient metal sites because NPs are prepared in solvents with pronounced electron donor activity, and they will compete with chalcogen atoms of

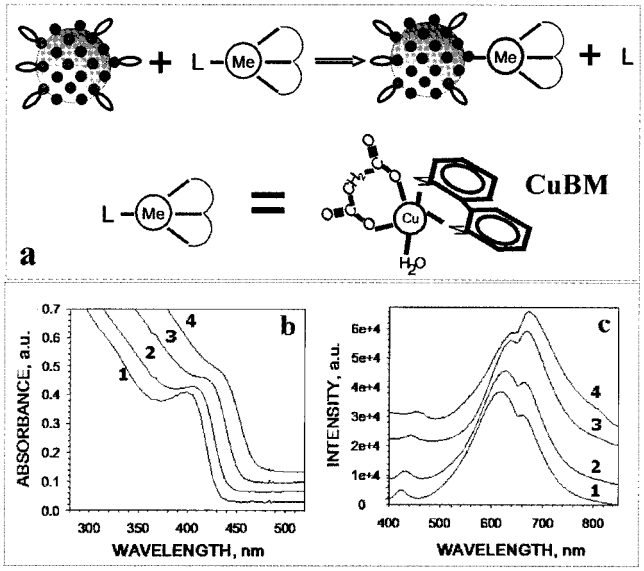

Figure 1. (a) Schematics of the chalcogen modification of II-VI semiconductor NPs with mixed ligand transition metal complexes. (b, c) Optical properties of CdS NPs stabilized with citrate: UV−vis absorption (b) and luminescence (c) spectra of CdS NPs. For traces 1, 2, 3, and 4 the synthetic ratio of Cd^{2+}/S^{2-} was 6:1, 4:1, 2:1, and 1:1, respectively.

NP for the reaction with Lewis acids. Therefore, quite mild − to avoid reaction with the stabilizer and the solvent − yet capable of binding to surface chalcogens Lewis acids must be used. They also must have an aromatic system or, more generally, p-conjugated system to make possible the spectroscopically legible electronic interaction between the electronic levels of NP and the modifier. In the capacity of a Lewis acid modifier satisfying these requirements, we used incompletely coordinated asymmetric metal complexes with labile ligands. In this case, the metal cation can act as an electrophile. The chalcogen centers on the NP surface are to replace the weak labile ligands, while the strong organic ligands will provide adequate molecular orbitals for the interaction with NP. The reaction of surface modification can be schematically depicted by Figure 1a.

As weak labile ligands, one can use monodentate inorganic ligands such as H_2O, NH_3, Cl^-, and others similar to them. The strong ligands can be bidentate organic molecules such as bipyridine, phenanthroline, and others. The metal complex used in this study is aqua(2,2′-bipyridyl-*N*,*N*′)(malonato-*O*,*O*′)-copper(II) monohydrate[18] (Figure 1a), which for brevity will be referred to as CuBM. The choice of this modifier was made on the basis of the strength of the Cu−S bonding and the spectral characteristics of CuBM, that are quite distinct and do not overlap with the band edge of the NPs, where spectral changes caused by the modification may occur.

The first attempts to study the chalcogen-modification reactions in II-VI semiconductor NPs according to the proposed scheme indicated that there were competitive reactions of the modifier with Lewis base-type of compounds, such as thiols or phosphines, used as stabilizers and/or as a solvent. This resulted in multiple side products and inconclusiveness of the spectral characteristics of the modification results. Hence, one should use a method of synthesis of the NPs stabilized by a relatively weak Lewis base, which would not react with metal complexes, yet producing fairly narrow size distribution. A successful synthetic recipe, which afforded suitable NPs, was found when

(26) Frisch, M. J.; Trucks, G. W.; Schlegel, H. B.; Gill, P. M. W.; Johnson, B. G.; Robb, M. A.; Cheeseman, J. R.; Keith, T.; Petersson, G. A.; Montgomery, J. A.; Raghavachari, K.; Al-Laham, M. A.; Zakrzewski, V. G.; Ortiz, J. V.; Foresman, J. B.; Cioslowski, J.; Stefanov, B. B.; Nanayakkara, A.; Challacombe, M.; Peng, C. Y.; Ayala, P. Y.; Chen, W.; Wong, M. W.; Andres, J. L.; Replogle, E. S.; Gomperts, R.; Martin, R. L.; Fox, D. J.; Binkley, J. S.; Defrees, D. J.; Baker, J.; Stewart, J. P.; Head-Gordon, M.; Gonzalez, C.; Pople, J. A. *Gaussian 94*, revision E.2; Gaussian, Inc.: Pittsburgh, PA, 1995.

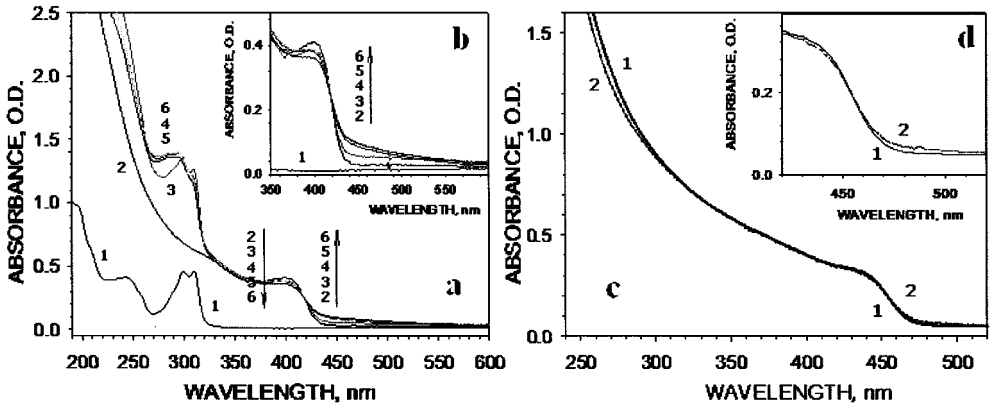

Figure 2. (a, b) Reaction of CuBM surface modification of CdS NPs monitored by UV−vis absorption spectroscopy. The NP:CuBM molecular ratio is 1:60. Spectra of individual reactants CuBM (1) and CdS (2) are given in conditions identical to those in the reaction mixture. Traces 3, 4, 5, and 6 are the UV−vis spectra of the reaction mixture 5, 10, 20, and 40 min after the beginning of surface modification. The reaction was carried out under ambient conditions and room temperature. Insert (b): the enlargement of the band-edge region of NPs. (c, d) UV−vis adsorption spectra of CdS NPs before (1) and after (2) addition of $CuCl_2$ solution. The molar ratio of NP:Cu^{2+} is 1:60. Insert (c): the enlargement of the band-edge region of NPs.

citrate ions were used as a stabilizer. The three carboxyl groups of citrate ions do not form as strong of individual covalent bonds with transition metals as thiols do, while acting together they are still capable of arresting the growth of NPs.[27,28] Here, we used thioacetamide as a sulfide source instead of sodium sulfide used previously in the synthesis of citrate-stabilized CdS.[28] Being initiated by heating with the microwave irradiation, decomposition of the thioacetamide results in the fast and uniform formation of sulfide ions in the bulk of the solution, which promotes simultaneous birth of numerous nucleation centers and, therefore, the formation of particles with relatively narrow size distribution.[29] The spectral characteristics of the obtained CdS NPs are given in Figure 1b,c. The increase of Cd^{2+} concentration results in the reduction of particle size, which can be understood as the result of the increase of NP surface charge and related to that electrostatic adsorption of citrate stabilizer. The particle diameter can be varied from ca. 26 to 44 Å, which is sufficient for the observation of size effects in the modified species. The emission properties are dominated by the trapped emission luminescence with maximum shifting from 620 to 670 nm as NP diameter increases (Figure 1c). The excitonic emission is weak, as is common for uncoated CdS NPs. Nevertheless, it is still easily recognizable in the peak in the blue part of the spectrum, which varies between 425 and 455 nm for the available particle diameters. The quantum yield of the trapped and excitonic emission bands is 6.0−7.5% and 0.15−0.15%, respectively. The NP of all sizes forms in the cubic crystal lattice as can be seen from the X-ray diffraction (Supporting Information Figure 1S), which is quite different from thiolic stabilizers promoting crystallization of CdS in hexagonal form.[17]

The modification of CdS NPs is achieved by mixing aqueous solutions of CdS and CuBM at room temperature. The course of the reaction can be monitored by UV−vis spectrophotometry (Figure 2 a,b) and by ESR (Figure 3). The reaction comes to completion within 40 min as can be seen by the cessation of spectral changes (Figure 2a,b), for example, spectral shifts in

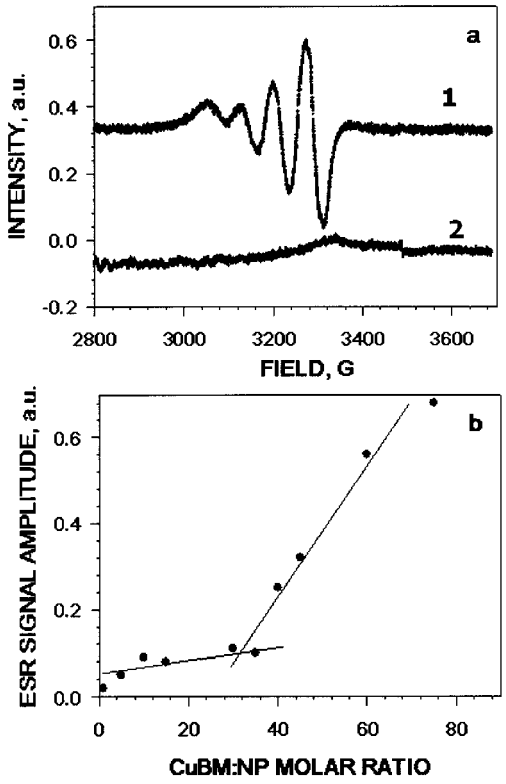

Figure 3. (a) Electron spin resonance spectra of CuBM before (1) and after (2) the addition of 34 Å CdS NPs in a NP:CuBM molar ratio of 1:25. (b) Dependence of ESR signal amplitude on CuBM:NP molar ratio during the surface modification reaction.

250−320 nm and 380−470 nm spectral regions. For a comparative study revealing the effect of organic ligands attached to the transition metal for surface modification, the similar UV−vis adsorption transients were collected for the reaction of CdS NPs with $CuCl_2$ (Figure 2c,d). Virtually no change in the 300−500 nm region, which includes several first excitonic transitions of NPs, is observed. This is an obvious difference from the results of surface modification of NP by the metal complex (Figure 2a,b).

Concomitantly with the changes in UV−vis spectra, the distinct ESR signal of Cu(2+) ion in CuBM disappears within 20−30 min after the beginning of the reaction (Figure 3a, trace

(27) Rogach, A. L.; Nagesha, D.; Ostrander, J. W.; Giersig, M.; Kotov, N. A. *Chem. Mater.* **2000**, *12*, 2676−2685.
(28) Correa-Duarte, M. A.; Giersig, M.; Liz-Marzan, L. M. *Chem. Phys. Lett.* **1998**, *286*, 497−501.
(29) Peng, X. G.; Wickham, J.; Alivisatos, A. P. *J. Am. Chem. Soc.* **1998**, *120*, 5343−5344.

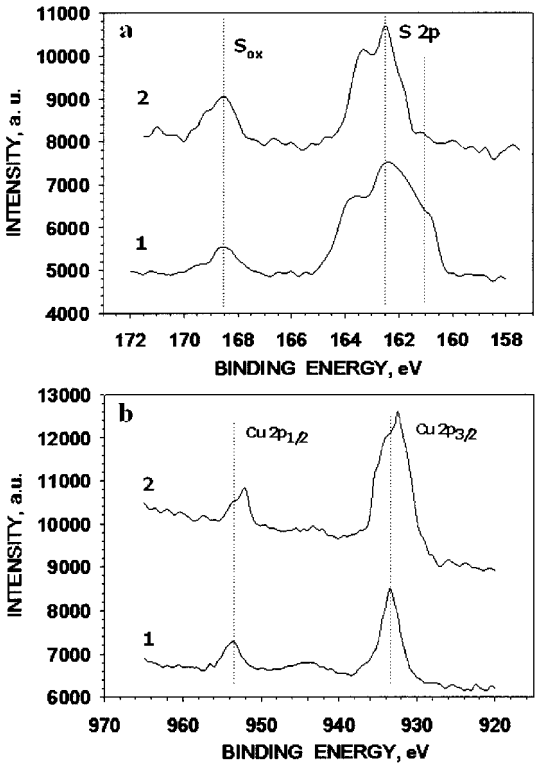

Figure 4. XPS spectra of sulfur (a) and copper (b) bands before (1) and after (2) CuBM modification of CdS nanoparticles.

2), which corresponds to the reduction of Cu(2+) to Cu(+1). This feature of the process is very convenient for the investigation of the surface modification because it affords structural data about the product from ESR and NMR. The dependence of the ESR signal versus the amount of the CuBM added (Figure 3b) has a distinct inflection point at a specific molar ratio between CuBM and CdS NPs (Figure 3b). The molar amounts of NP were calculated assuming the average number of CdS units in 34 Å spheres with spectral characteristics as presented in Figure 2a,b equal to 400. Considering the linear rise of the ESR signal for higher concentrations of CuBM, that is, increasing amount of unreacted Cu(2+) in the sample, the inflection point corresponds to the saturation of the capacity of the NP surface by the modifying groups.

The nature of the chemical processes taking place between CdS NPs and CuBM can be also probed by X-ray photoelectron spectroscopy (XPS). The XPS spectrum is fairly complex. This is due to the presence of sulfur in different electronic environments in NPs. The bands of sulfur and copper atoms were in the focus of our attention as they provide the most direct information about the new bond(s) forming in the reaction (Figure 4). S 2p and Cu $2p_{3/2}$ XPS bands of both sulfur and copper located at 160−163 eV and 930−938 eV, respectively, have complex shapes produced by superposition of several peaks corresponding to atoms in different electronic states. Importantly, the shoulder of the sulfur peak at 161 eV disappears after the modification, which is also accompanied by the increase of the signal from oxidized sulfur at 168.5 eV (Figure 4a). At the same time, the maximum of the Cu $2p_{3/2}$ signal shifts from 933.5 to 932.5 eV, which is also mirrored by the change in the Cu $2p_{1/2}$ band moving from 953.5 to 952.0 eV (Figure 4b).

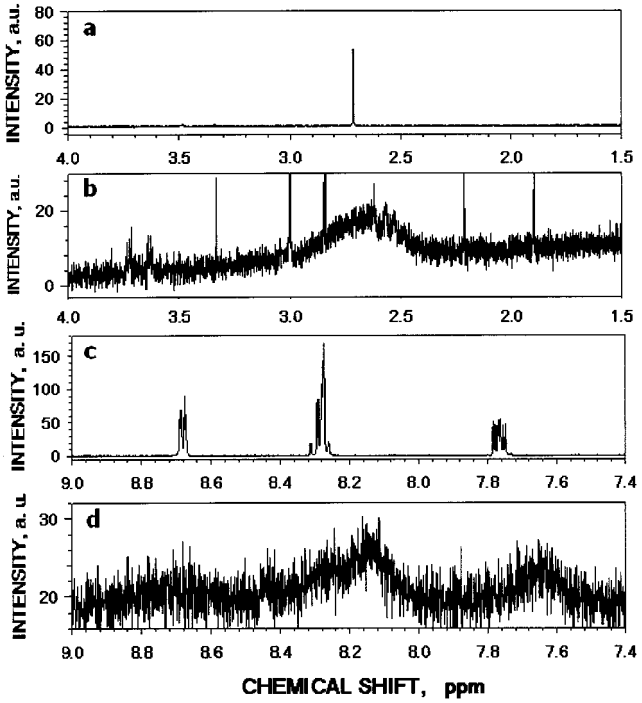

Figure 5. NMR spectra of malonic acid (a), modified CdS NPs with NP:CuBM molar ratio of 1:40 (b), protonated bipyridine, pH = 1 (c), and modified CdS NPs with NP:CuBM molar ratio of 1:60 (d). All spectra have been taken in D_2O.

The NMR data of the reaction product are presented in Figure 5. The unreacted paramagnetic CuBM complex is not visible by this spectroscopy, and, therefore, one can see only the signals from reduced CuBM units attached to NPs. After the modification, one can see the NMR bands in the spectral regions characteristic for malonic acid (Figure 5a) and protonated bipyridine (Figure 5c). However, the new bands are significantly broadened and slightly shifted upfield. Importantly, no free malonic acid or bipyridine with significantly stronger and narrower signals could be seen upon the completion of the modification reaction.

The size distribution before and after the modification can be assessed by TEM, and the corresponding data and images are presented in Supporting Information (Figure 2S). A TEM diameter of 3.3 nm correlates very well with the one estimated from the position of the UV−vis absorption band and literature data.[17] The reaction of CdS and CuBM does not change the diameter of the NP's cores remaining at 3.3 nm.

Considering diverse emission properties of transition metal complexes and Cu(I) ions themselves, one could expect substantial modification of the luminescence pattern of NPs upon the attachment of CuBM. Indeed, the emission spectra are found to be quite different from those for parent NPs, and they also depended on the region where the product is excited. For 290 nm excitation wavelength, we see the appearance of a new band at 360 nm for CuBM-modified NPs (Figure 6a). For 340 nm excitation light, a new band at 445−450 nm is observed (Figure 6b). Simultaneously, a decrease of intensity and red spectral shift of the trapped emission of NPs at 600−700 nm occur. The lifetimes of the emission at different wavelengths are given in Table 1.

The variation of the ionic conditions during CdS NPs synthesis affords the variation of particle size allowing the

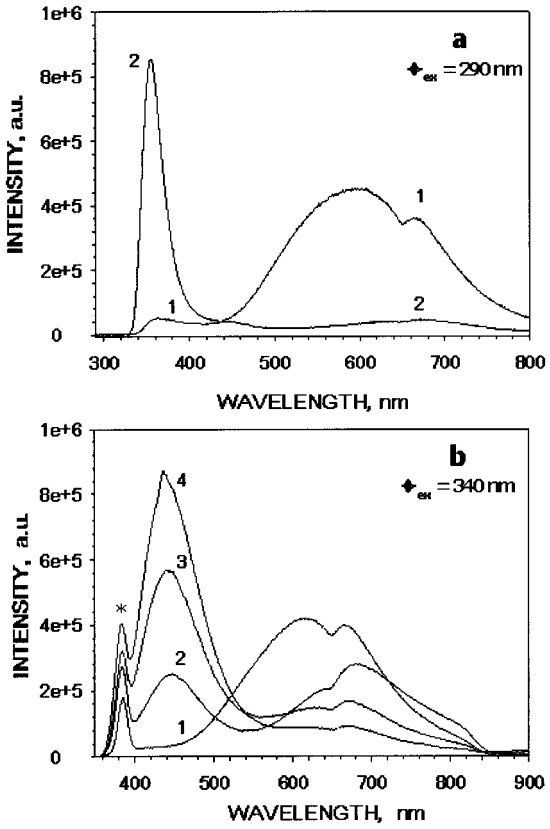

Figure 6. (a) Luminescence spectra of the modified CdS NP excited at 290 nm before (1) and after (2) the reaction with CuBM (NP:CuBM molar ratio is 1:60). (b) Luminescence spectra of the modified CdS NP excited at 340 nm before (1) and after (2, 3, 4) the reaction with CuBM. Traces 2, 3, and 4 correspond to NP:CuBM molar ratios of 1:20, 1:40, and 1:60, respectively.

Table 1. Lifetimes of NP Emission in Different Parts of the Spectrum Obtained by Time-Correlated Single Photon Counting

	lifetime (ns)				
samples	350 nm	414 nm	447 nm	580–620 nm	651–660 nm
CdS (nonmodified)		18.7 ± 2		64.3 ± 3	78.0 ± 4
CdS-CuBM, 1:20	10.5 ± 1.5		5.3 ± 0.7	115 ± 5	131 ± 8
CdS-CuBM, 1:40			5.4 ± 1.1	104 ± 8	128 ± 15
CdS-CuBM, 1:60			4.8 ± 0.5	96 ± 10	102 ± 12
CdS-CuBM, 1:80	10.4 ± 2		4.6 ± 0.75	110 ± 11	115 ± 13

investigation of the quantum size effect on the luminescence properties of the modified NPs. As one can see from Figure 7a, the new luminescence bands at 445−450 nm and 600−700 nm do not depend on particle size.

The excitation spectra of the red luminescence band for original and modified NPs are given in Figure 7b. A very strong new peak appears at 300 nm after the attachment of CuBM to CdS, while the features in the 350−500 nm region coincide with those of naked NPs.

To help understand the optical changes in the modified NPs, the quantum chemical modeling of the NP surface was carried out by using semiempirical PM3 and DFT algorithms. Most of the data were calculated at the p-BP86/DN(*)//PM3 level of theory. On the basis of the structural information obtained from UV−vis, ESR, and NMR data discussed below, the modified NPs are simulated by an elementary cell of cubic CdS (in accord with X-ray diffraction data with attached CuBM unit) presented in Figure 8a. The model consists of four Cd and four S atoms with one of the S atoms in the cube being bound to the Cu center in the (2,2′-bipyridyl-*N*,*N*′)(malonato-*O*,*O*′)-copper moiety. The calculated molecular orbitals for this model cluster describe the new surface states of the CuBM-modified NP.

The dangling bonds of sulfur atoms on the left side of the cluster representing the interface with atoms of the crystal lattice inside the NP were closed with CH_3 groups. These endgroups were chosen instead of simpler hydrogen capping to avoid artificial intramolecular hydrogen bonding which would distort both the geometry and the electronic orbitals of the cluster. In the calculation algorithm, we used the Becke−Perdew exchange-correlation functional, which provides reliable results for both occupied and unoccupied states. The occupied and empty electronic states are denoted here as HOMOs and LUMOs, respectively, with HOMO 1 and LUMO 1 being the frontier orbitals. Among the molecular orbitals calculated, there are the electronic states enveloping the atoms of both the NP surface and the modifier exemplified by LUMO 1 and HOMO 1(Figure 8b,c). HOMO 6 (Figure 8h), HOMO 7, HOMO 8, and LUMO 10 (not shown) also display this property. The distribution of electron density in the orbitals reflects the involvement of different parts of the complex and the surface of the NP. It was noted that LUMOs tend to concentrate on the predominantly aromatic bipy part of the CuBM moiety, while HOMOs are more often localized on the CdS part. The sequence of the LUMOs and HOMOs provides insight into the photophysics of the modified NPs revealing possible excitation relaxation pathways of electrons and holes, respectively, which will be used when discussing the luminescence data.

Independent information about the occupied energy levels in the naked and CuBM-modified NPs can be obtained from ultraviolet photoelectron spectroscopy (UPS) data (Figure 9). The signal intensity in UPS is proportional to the total amount of electrons ejected from NPs by illumination with 21.2 eV UV light. A part of the energy of the absorbed UV quantum is spent on the overcoming of the forces binding the electron to the molecule (ionization potential), while the rest is released as the kinetic energy of electron measured by the instrument. The UPS spectrum is plotted with abscissa expressed in units of binding energy. The onset of the signal, that is, binding energies of 8−10 eV, represents the electrons ejected from the valence band of the semiconductor, while the positions of maximums correlate with the energy of other electronic states.

Discussion

1. Structure of the Chalcogen-Modified CdS Nanoparticles. Before the discussion of the optical properties of CuBM-modified CdS NPs, some structural information about the product of the reaction in Figure 1a needs to be established. The ESR spectra (Figure 3a) unequivocally demonstrate the reduction of the copper metal center of CuBM. The disappearance of the ESR signal indicates the transition from the paramagnetic $3d^9$ state of Cu(2+) to the ESR-invisible diamagnetic $3d^{10}$ state Cu(1+). Such a reaction is typical for binding of Cu(2+) to various thiols and other sulfur-containing groups[30,35] including CdS NPs.[31]

(30) (a) Rorabacher, D. B.; Martin, M. M.; Koenigbauer, M. J.; Malik, M.; Schroeder, R. R.; Endicott, J. F.; Ochrymowycz, L. A. Structural Effects on Cu(II)/Cu(I) Potentials and Electron Transfer Kinetics as well as Related Physical Properties in Polythiaether and Polyaminothiaether Complexes. In *Copper Coordination Chemistry*: *Biochemical & Inorganic Perspectives*; Karlin, K. D., Zubieta, J., Eds.; Adenine Press: Guilderland, New York, 1983.

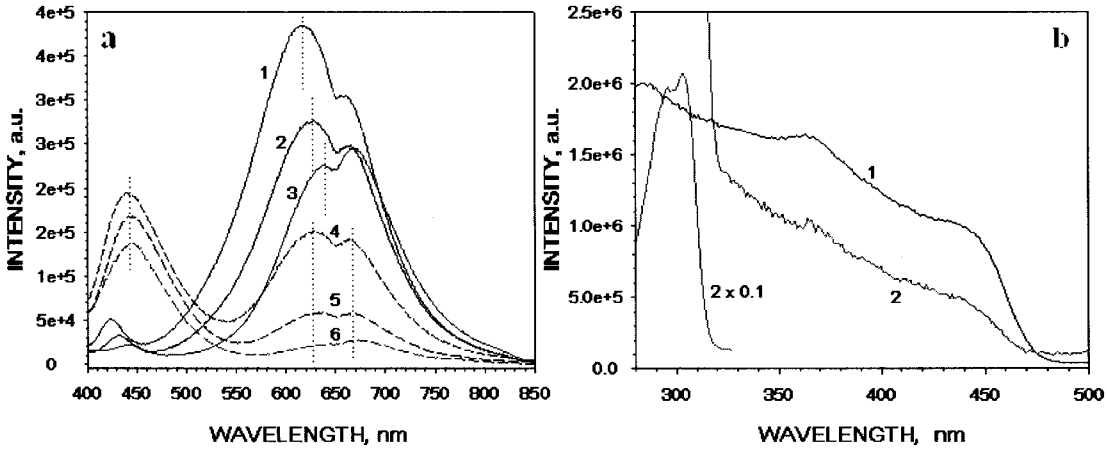

Figure 7. (a) The effect of particle size on luminescent properties. Luminescent spectra of CdS NPs with gradually increasing diameter before (1, 2, and 3) and after (4, 5, and 6) the modification with CuBM (NP:CuBM molar ratio is 1:60). (b) Excitation spectra registered at 670 nm for CdS NPs before (1) and after (2) the modification with CuBM (NP:CuBM molar ratio is 1:60). Trace 2 × 0.1 was scaled down 10 times as compared to trace 2 to reveal the features of the 300 nm peak.

The core electron binding energies positions of the XPS signals of copper and sulfur were shown to directly correlate with atomic charges on these atoms.[32] This can be used to elucidate the important structural information about the CuBM-CdS complex (Figure 4). Cu and S bands are the only components of the XPS spectra that significantly change their positions. As expected, the redox reaction here occurs between the copper and sulfur atoms. The Cu $2p_{3/2}$ and $2p_{1/2}$ signals shift to lower binding energies (Figure 4b), which is also accompanied by the weakening of the satellite peak at 944 eV. This confirms the ESR data regarding the Cu(2+) → Cu(1+) redox transition.[33] One can also see the simultaneous shift of the S 2p band to higher binding energies (Figure 4a) and an increase of the peak intensity at 168.5 eV corresponding to the oxidized forms of sulfur. Interestingly, the S 2p band has a lot of components contributing to the XPS band. The one that disappears after the modification is the low binding energy component at 161 eV and is attributed to the highly electron-donating sulfur states with dangling bonds located on the surface of NPs.[34] Other sulfur states with binding energies between 162 and 164 eV are most likely located in the interior of NPs and remain unchanged. Thus, these internal sulfur sites are not involved in the reaction.

The chemistry of copper ions and various sulfur organics is well studied due to its biological significance. As substantiated by abundant literature on the subject,[30,35,36] the reduction of Cu(2+) complexes by thiols and similar species always leads to Cu−S covalent bonding. The formation of the Cu−S bond is accompanied by restructuring of the coordination sphere of the metal and replacement of the weaker/harder ligands because of the high affinity of these atoms to each other characterized as soft Lewis acids and soft Lewis bases. In the view of ligand exchange, it is interesting to analyze the UV-spectra of the CdS-CuBM adduct. Let us compare the UV−vis absorption spectra of the metal complex, CdS NPs, and the modification reaction product (Figure 2a,b). The characteristic peaks at 300 and 310 nm of CuBM correspond to the ligand-to-metal charge transition from the p-levels of bipyridine and malonic acid ligands to the top d-level and s-level of copper atom.[37] The energy of the vacant level depends on the ligand field generated by water and other ligands and the Jahn−Teller splitting of d-levels in copper. The 300/310 nm peaks of CuBM undergo a blue shift producing a combination band at 285 nm after reaction with CdS NPs. The similar but stronger blue shift from 300/310 nm to 275 nm can be seen for the reaction of CuBM with Na_2S (Supporting Information Figure 3). In the spectrochemical series of metal complexes, the ligand field increases in the order of H_2O > $R-S^-$ > S^{2-}, which correlates very well with the observed evolution of the ligand-to-metal charge transition 300/310 nm → 285 nm → 275 nm. Thus, the ligand strength of sulfur sites on the NP surface can be compared to that of $R-S^-$, which matches the XPS data (Figure 4a). Note that these considerations are not affected by the fact that there is an additional blue shift due to the reduction of the metal center.

Summarizing the ESR, XPS, and UV−vis data, they essentially show that copper atoms bearing some organic moiety become covalently attached to the NPs. Additional information about the structure of the molecular unit bound to the NP surface can be obtained from NMR experiments in Figure 5. The paramagnetism of unreacted CuBM helps this study because it makes free CuBM NMR-silent, and therefore its lines do not interfere with those from modified NPs when Cu is in the (1+) state. In Figure 6b,c, one can see that the NMR signals of malonic acid ligand (Figure 5b) and bipyridine ligand (Figure 5d) are broadened and shifted in the product of the modification reaction as compared with the solutions of the same substances in D_2O. The broadening and shifts are consistent with the data for liquid NMR spectra of thioglycerol[38] and thiophenol moieties

(31) Izarov, A. V.; Chrysochoos, J. *Langmuir* **1997**, *13*, 3149.
(32) Larsson, R.; Folkesson, B. *Acta Chem. Scand.* **1991**, *45*, 567−571.
(33) Larsson, R.; Folkesson, B. *Acta Chem. Scand.* **1991**, *45*, 567−571. Li, B.; Xie, Y.; Huang, J.; Qian, Y. *J. Solid State Chem.* **2000**, *153*, 170−173. Laajalehto, K.; Leppinen, J.; Kartio, I.; Laiho, T. *Colloids Surf., A* **1999**, *154*, 193−199.
(34) Kartio, I. J.; Basilio, C. I.; Yoon, R.-H. *Langmuir* **1998**, *14*, 5274−5278.
(35) Brader, M. L.; Borchardt, D.; Dunn, M. F. *J. Am. Chem. Soc.* **1992**, *114*, 4480−4486. Itoh, S.; Nagagawa, M.; Fukuzumi, S. *J. Am. Chem. Soc.* **2001**, *123*, 4087−4088. Vaher, M.; Romero-Isart, N.; Vasak, M.; Palumaa, P. *J. Inorg. Biochem.* **2001**, *83*, 1−6. Sung, M. M.; Sung, K.; Kim, C. G.; Lee, S. S.; Kim, Y. J. *Phys. Chem. B* **2000**, *104*, 2273−2277. Smith, R. C.; Reed, V. D.; Hill, W. E. *Phosphorus, Sulfur Silicon Relat. Elem.* **1994**, *90*, 147−154.
(36) Janssen, M. D.; Grove, D. M.; Van Koten, G. *Prog. Inorg. Chem.* **1997**, *46*, 97−149.
(37) Schugar, H. J. Ligand to Metal Charge-Transfer Spectra of Cu(II) Chromophores. In *Copper Coordination Chemistry: Biochemical & Inorganic Perspectives*; Karlin, K. D., Zubieta, J., Eds.; Adenine Press: Guiderland, New York, 1982; pp 43−74.

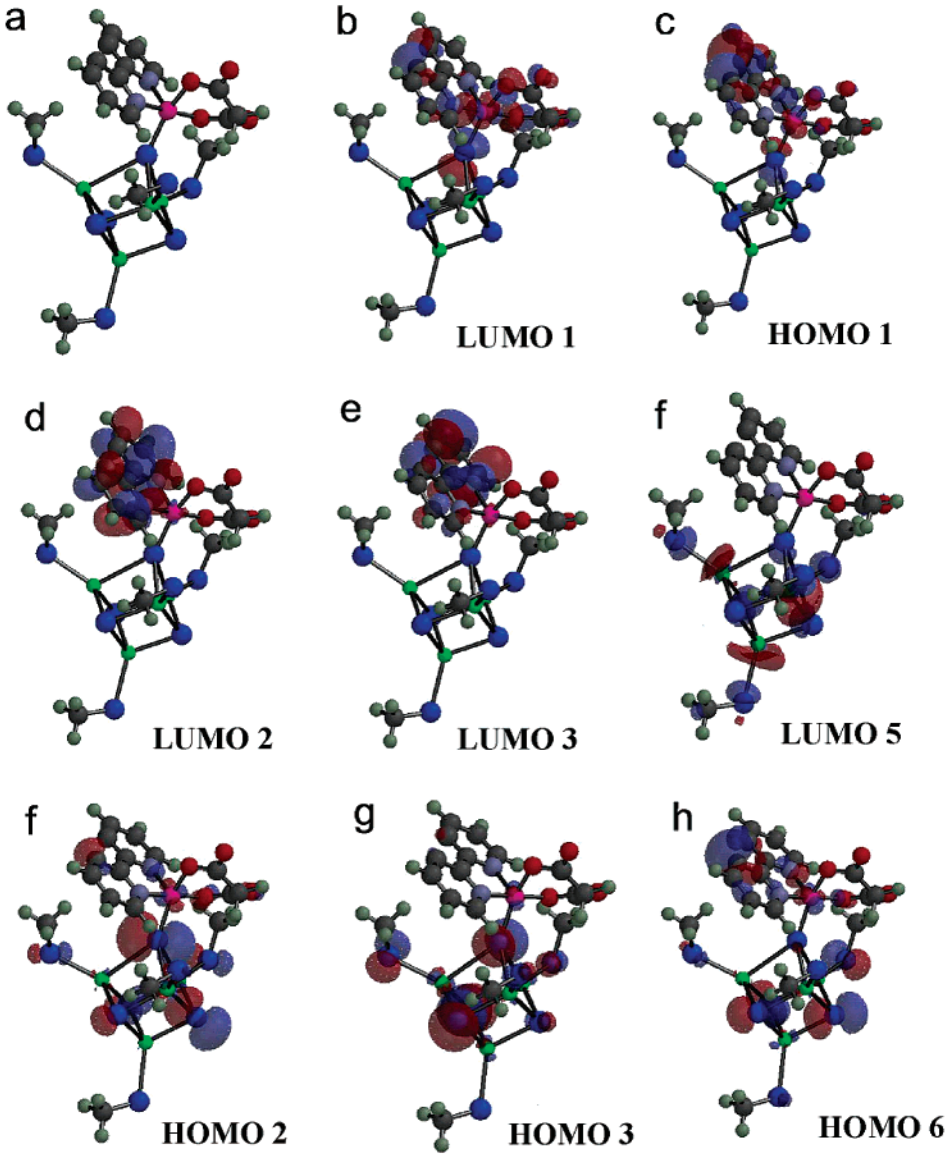

Figure 8. Molecular orbitals of CdS-CuBM model cluster computed at the p-BP86/DN(*)// PM3 level of theory. Atoms are color coded as follows: Cd (green), S (blue), Cu (magenta), C (dark gray), H (light gray), N (yellow), and O (red). The positive and negative regions of the orbitals are depicted as red and blue clouds.

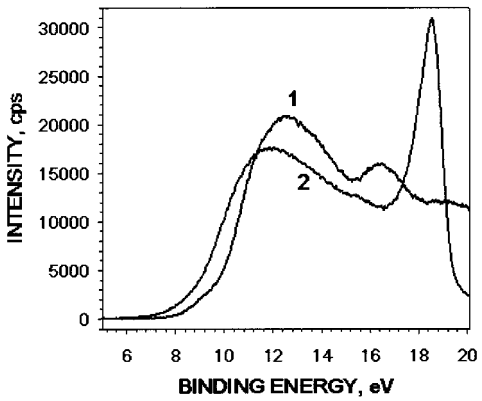

Figure 9. UPS spectra of 34 Å nanoparticles before (1) and after (2) the modification with CuBM. All energies are referenced to the energy of an electron in a vacuum.

attached to CdS.[39] The broadening of the NMR lines is attributed to the frustration of rotational and vibrational moment of the attached organic groups when adsorbed to heavy NPs with slow tumbling, which can also be seen for thiol-stabilized CdS[38] and gold NPs.[40] Importantly, no signal from *free* malonic acid or bipyridine ligands can be seen, although they are supposed to be much stronger than the NMR lines from the same ligands bonded to the NPs. This lack of signal proves that the complex of the transition metal with both bidentate ligands remains intact.

The average number of CuBM moieties attached to a NP can be determined from the dependence of ESR signal on the CuBM concentration (Figure 3b). The position of the inflection point in the dependence of the ESR signal on the CuBM concentration shows the point when the capacity of the NP surface for CuBM binding becomes saturated. From this, one can calculate that ca. 30−40 units are bound to the NP surface. This is an upper estimate of the total number of attached groups since some part

(38) Nagesha, D. K.; Liang, X.; Mamedov, A. A.; Gainer, G.; Eastman, M. A.; Giersig, M.; Song, J. J.; Ni, T.; Kotov, N. A. *J. Phys. Chem. B* **2001**, *105*, 7490−7498.
(39) Sachleben, J. R.; Wooten, E. W.; Emsley, L.; Pines, A.; Colvin, V. L.; Alivisatos, A. P. *Chem. Phys. Lett.* **1992**, *198*, 431−436.
(40) Badia, A.; Cuccia, L.; Demers, L.; Morin, F.; Lennox, R. B. *J. Am. Chem. Soc.* **1997**, *119*, 2682−2692.

of CuBM may react with sulfide ions always present in CdS dispersion. Considering that there are approximately 120 surface atoms of sulfur in tetrahedral 34 Å CdS NP, the decoration with CuBM is rather selective because of (1) differences in nucleophilic character of different sulfur atoms on the NP surface in different atomic environments (see XPS spectra) and (2) the spatial constraints for accommodating the bulky metal complex units. Therefore, the structure of the product of the modification reaction in Figure 1a can be described as a few tens (<40) of (2,2′-bipyridyl-*N*,*N*′)(malonato-*O*,*O*′)-copper units attached via a Cu−S bond to the surface of NPs. The total number of the decorating metal complexes may, of course, vary depending on the amount of CuBM added and the diameter of the NP. In perspective, the reduction of the overall number of the metal complex units bound to the NP may be desirable for the synthesis of multiparticle associates, while the increase of the modifier density will be beneficial, for instance, in catalysis.

Overall, the CuBM-modified NP can be considered as a member in the new family of the supramolecular compounds on the basis of transition metal complexes with two qualitatively different chromophores united in one structure.[41] Similarly to bipyridine-based molecular constructs,[42] one may expect new optical effects in the NP supramolecule stemming from the electronic interaction between the chromophores.

2. Optical Properties. 2.1. Absorption Spectra. In the course of the modification reaction, the broadening of the UV−vis absorption edge of the nanoparticles in the 400 nm spectral region is observed (Figure 2a,b), which brings about the question regarding the nature of this effect. Several possibilities have been considered such as light scattering, the increase of particle size, and the formation of a thin shell made of narrow band gap semiconductor. As can be seen from the statistical analysis of multiple TEM images, there is no significant change of the NP core size or size distribution, which may produce such broadening (Supporting Information Figure 3S). The dynamic light scattering also did not reveal any change in particle aggregates after the CuBM modification, thereby removing scatter broadening from the possible suspects causing the red shift. CuS or Cu_2S deposits on CdS, formed due to the breakdown of the transition metal complex, may theoretically give rise to the similar effect in UV−vis absorption spectra. However, the complex decomposition is frustrated by the complexation of copper(II) with bidentate ligands, and there are no NMR indications of this process occurring (Figure 5). Moreover, even when CdS dispersion is exposed to $CuCl_2$ solution in the NP:Cu^{2+} ratio of 1:60 *equimolar* to that used for the decoration of NPs with CuBM, the changes in the UV-spectrum are barely visible in the entire spectral range (Figure 2c,d), which rules out the copper sulfides deposits as a source of broadening.[43] The comparison of traces 2 and 6 in Figure 2a,b indicates that the CuBM modifier affects the light absorbing properties of NPs. However, the effect is small because they are mostly determined by the transitions in the NP core. The wave functions of both electron and hole for the first excitonic transition in this size range are concentrated mainly in the center of the NP and, therefore, are difficult to influence by changing the surface states except for the case of very small CdS clusters as observed in ref 6.

The discussion of adsorption properties of the CuBM-modified CdS brings about an important question regarding the interaction between the surface modifier and NPs. While there are both experimental[6,8−12,44,45] and theoretical[12] evidence of the electronic communication between aromatic modifiers and II-VI semiconductor clusters in the structures studied previously, these effects remain difficult to observe by UV absorption spectroscopy. One of the reasons is the difficulty of shifting the energy of the core levels of NP, which are mainly determined by crystal lattice of the semiconductor NP in the interior rather than by the exterior atoms and the interference from other processes such as scattering. To some extent, this problem may be alleviated by sharpening the size distribution of the NPs. This can be done by using stronger stabilizers, which, however, will interfere with Lewis acid modification (see Results). On the other hand, the luminescence properties of NP are dramatically affected by the surface atoms because the surface states change the electron/hole recombination pathways. Therefore, before discussing the fluorescence spectra, it would be necessary to consider the electronic structure of the CuBM-modified NPs.

2.2. Surface Electronic Structure. In our previous paper,[19] we found that the surface of modified CdS NPs could be locally modeled as a small CdS cluster. Infrared spectra were simulated for them and were in good agreement with the experimental data. Additionally, the quantum mechanical modeling helped us to clarify the origin of some of the IR peaks of naked NPs. Encouraged by these results, we used similar PM3 and DFT algorithms in this work, to provide clues about the electronic structure on CuBM-modified CdS and, ultimately, to understand their emission properties. The atomic structure of the surface states on the modified NPs can be described by the model cluster Figure 8a. Different molecular orbitals corresponding to this cluster unveil how the surface of CdS cluster and the transition metal complex modifier interact in the prepared supramolecules. What seems to be an important and novel feature of the electronic structure is the formation of *delocalized* unoccupied and occupied molecular orbitals enveloping the surface atoms of CdS, copper atom, the organic ligands of the transition metal complex, such as LUMO 1, HOMO 1, HOMO 6, and others (Figure 8b,c,h). Apparently, the delocalized molecular orbitals are characteristic for the chalcogen modification of NPs with metal complexes because similar calculations done for cubic CdS cluster with thiophenyl moiety attached to one of the Cd atoms (Figure 10-1) did not reveal any hint of bridging orbitals involving the π-system of the phenyl ring. Such orbitals are also not seen for a bigger model $Cd_{10}S_4(SPh)_{16}^{4-}$ that closely resembles small NPs with large number of aromatic phenyl rings (Figure 10-2). There is a clear demonstration that no d-orbitals of Cd atoms are involved in the formation of the corresponding HOMOs or LUMOs, as was expected from the fact that they are fully occupied (see Introduction).

The difference in molecular orbitals obtained for chalcogen and metal anchoring of aromatic molecules originates in the availability and overlap difference of the atomic orbitals forming

(41) Sauvage, J. P.; Collin, J. P.; Chambron, J. C.; Guillerez, S.; Coudret, C.; Balzani, V.; Barigelletti, F.; De Cola, L.; Flamigni, L. *Chem. Rev.* **1994**, *94*, 993−19.
(42) Balzani, V.; Juris, A.; Venturi, M.; Campagna, S.; Serroni, S. *Chem. Rev.* **1996**, *96*, 759−833.
(43) A similar reaction when copper sulfides did form under excess of sulfide was studied in ref 31.
(44) Veinot, J. G. C.; Galloro, J.; Pugliese, L.; Pestrin, R.; Pietro, W. J. *Chem. Mater.* **1999**, *11*, 642−648.
(45) Schmelz, O.; Mews, A.; Basche, T.; Herrmann, A.; Muellen, K. *Langmuir* **2001**, *17*, 2861−2865.

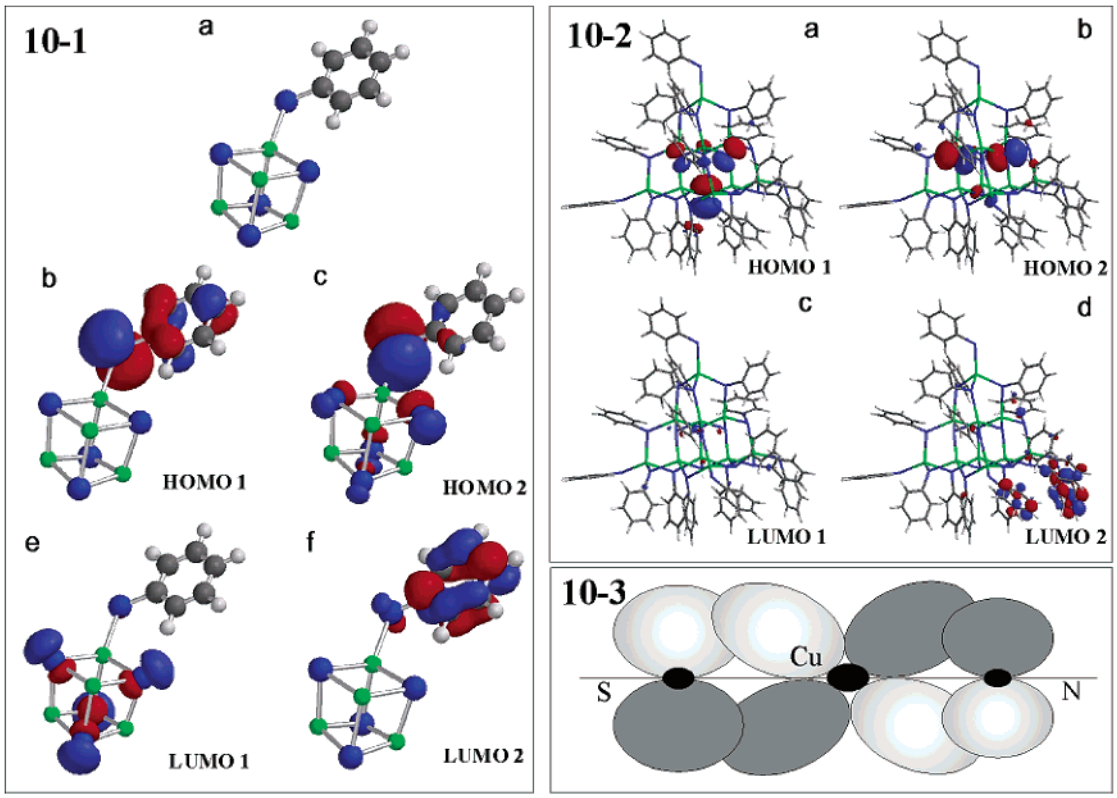

Figure 10. (10-1) Molecular orbitals of CdS-Phen model cluster computed at the PM3 level of theory. Atoms are color coded as follows: Cd (green), S (blue), C(dark gray), and H (light gray). The positive and negative regions of the orbitals are depicted as red and blue clouds. (10-2) Molecular orbitals of $Cd_{10}S_4(SPh)_{16}^{4-}$ small NP model computed at the PM3 level of theory. Atoms are color coded as follows: Cd (green), S (blue), C (dark gray), and H (light gray). The positive and negative regions of the orbitals are depicted as red and blue clouds. (10-3) Schematics of the butterfly bridging between p-orbitals of sulfur and p-orbitals.

the link between the NP and the modifier. In the CdS/CuBM supramolecule, the sulfur sites are capable of p-bonding via available p-atomic orbital carrying one electron on it after partial oxidation by Cu(2+). These p-orbitals overlap with a butterfly d-orbital of copper (Figure 8b,c,f). This can be observed for the frontier molecular orbitals HOMO 1 and LUMO 1 as well as for other molecular orbitals such as HOMO 2 (Figure 8b,c,f). At the same time, the butterfly d-orbital overlaps with the p-orbitals of nitrogen forming the aromatic system of bipyridine and oxygen atoms of the malonic acid in the fashion presented in Figure 10-3. Thus, the d-orbitals of the transition metal realize the bridging between the p-orbitals of sulfur on the surface of NP and the π-system of the aromatic ligands of the complex such as bipyridine. Moreover, the S−Cu−N atomic sequence is quite effective for the conjugation of the NP surface with organic aromatic systems because both parts are linked by one atomic orbital of the transition metal with very convenient symmetry and orientation for that purpose. Such a mode of bridging is certainly not available for Cd−S−C or Cd−N−C atomic groups present in NPs modified via Cd-atoms, because the middle atom has to engage orthogonal p-orbitals for the interaction with both parts of the system. Moreover, the mixing of p-orbitals of S and N with the butterfly d-orbitals of transition metal (Figure 10-3) diminishes the disparity in their energy levels.

The signature of the delocalized states is difficult to see in UV−vis absorption, but it can be seen in the UPS spectra of the modified NPs. The surface modification of CdS brings about significant change in its UPS spectrum (Figure 9, trace 2). A new strong band at 18 eV appears, while the other weaker one at 16.5 eV disappears. This clearly indicates reorganization in the electronic states upon addition of a (2,2′-bipyridyl-*N*,*N*′)-(malonato-*O*,*O*′)-copper unit to a NP. Additionally, the onset of the UPS signal, representing the top of the valence band of CdS, shifts to lower binding energies by approximately 1−9 eV in naked NPs and 8 eV in modified ones. The UPS peak also shifts by the same increment from 12.5 to 11.5 eV. Considering this shift, it is essential to note that the localized surface states of II-IV semiconductors have a very low photoelectron ejection cross section and typically cannot be seen when the sample is excited with a regular He UV light source used in this work. For the surface states, synchrotron UPS setups are normally used.[46] The delocalization involving aromatic systems of the new surface states should significantly increase their UPS cross section as compared to the parent states. The same effect in UPS spectra was observed for other chemical systems, where the transition from localized to delocalized molecular states occurred.[47−49] A strong increase of the UPS

(46) Magnusson, K. O.; Flodstroem, S. A. *Phys. Rev. B*: *Condens. Matter* **1988**, *38*, 6137−6142. Magnusson, K. O.; Flodstroem, S. A.; Maartensson, P.; Nicholls, J. M.; Karlsson, U. O.; Engelhardt, R.; Koch, E. E. *Solid State Commun.* **1985**, *55*, 643−647. Turowski, M.; Margaritondo, G.; Kelly, M. K.; Tomlinson, R. D. *Phys. Rev. B*: *Condens. Matter* **1985**, *31*, 1022−1027. Namba, H.; Nakanishi, N.; Yamaguchi, T.; Kuroda, H. *Phys. Rev. Lett.* **1993**, *71*, 4027−4030. Takahashi, T.; Ebina, A. *Appl. Surf. Sci.* **1982**, *11*−*12*, 268−287.
(47) Starnberg, H. I.; Nilsson, P. O.; Hughes, H. P. *Mater. Sci. Forum* **1992**, *91*−*93*, 727−732.
(48) Osterwalder, J.; Greber, T.; Aebi, P.; Fasel, R.; Schlapbach, L. *Phys. Rev. B*: *Condens. Matter* **1996**, *53*, 10209−10216.
(49) Orlowski, B. A. *Surf. Sci.* **1988**, *200*, 144−156.

signal intensity from the surface states was also seen for many adsorbates.[50,51] Hence, the red shift is attributed to the appearance of delocalized occupied electronic levels such as HOMO 1, formed from previously invisible electron donor sites, such as S^-. Both of them remain in the mid band gap region, which is reflected by the lower onset of electron ejection.

2.3. Luminescence Properties. Because we now have some information about the electronic structure of the prepared supramolecules, it becomes easier to discuss their luminescence properties. They strongly depend on the surface processes, and, indeed, one can see dramatic change in the emission pattern, which bears little resemblance with any modified NPs studied previously. There are two new emission bands at 350 and 414 nm, while the broad band of the red luminescence at 600−700 nm shifts to 630−750 nm. At the moment, the discussion of new bands at 350 and 414 nm will be contained to a very brief account, to avoid misinterpretations of results that will follow. (1) Short lifetimes of the new emission bands at 350 and 447 nm indicate that they are not *regular* d−d emissive transitions of copper ions, that are known to be forbidden and have lifetimes >10 μs.[52] (2) The 447 nm peak is not an enhanced excitonic band of the NPs, although it is located in the same spectral region, and its lifetime coincides with those previously reported for excitonic electron/hole recombination.[53] The reason for this conclusion is the fact that the position of the new band does not depend on the particle size as can be seen from Figure 7a, which should be expected for the CdS excitonic emission.

Because we are interested in the effects occurring on the NP surface, the major focus of the discussion will be placed on the luminescence of NPs at 600−700 nm. This band is typically attributed to the emission of the charge carriers trapped in the surface states undergoing the recombination between themselves and/or with the carriers on the conduction and valence bands. What is quite peculiar about this luminescence is that its lifetime increased from 64−78 to 110−115 ns after reaction with CuBM, while the overall intensity decreases. This contradicts the common scheme of dynamic luminescence quenching of NPs when both intensity and the lifetime decrease due to more intense nonradiative processes.[54] In some instances, such as static quenching, the lifetime may remain the same for the quenched electronic state being determined by unassociated with quencher molecules, but it never increases.[54] The fact of lifetime elongation was also confirmed by additional experiments on a completely different time-resolved luminescence system based on phase modulation, which gave similar results; the lifetime of the dominant component (>50%) of emission >520 nm increases from 43 to 170 ns for nonmodified CdS and for CdS-CuBM 1:20 complex, respectively. This observation also has no analogies in data obtained for other NP-dye assemblies reported so far; the lifetime of NP red emission inevitably decreased as a result of electron and/or Föster energy transfer quenching.[55]

We believe that the explanation for the effect of lifetime elongation can be found in the formation of the delocalized electronic states. The new HOMO 1 and LUMO 1 levels of CuBM-modified CdS surface (Figure 8b,c) are likely to be located between the valence and conduction bands of CdS, which correlates well with the UPS data (Figure 9). Therefore, they can be populated by the adsorption of the excitonic states of the NP core. The confirmation for that can be clearly seen in the excitation spectrum of this band in the region 350−500 nm (Figure 7b, trace 2), which coincides very well with the absorption spectrum of the unmodified NP repeating all its features (Figure 7b, trace 1). The energy gap calculated for HOMO 1and LUMO 1 presented in Figure 8 by DFT algorithm is 1.5 eV. This is also very close to the energy of the observed red emission of supramolecules; the energy of 700 nm light quantum is 1.76 eV. The 630−750 nm luminescence band also does not show any pronounced size dependence (Figure 7a) as opposed to the red luminescence of the naked NPs. Altogether, these facts lead to the conclusion that 630−750 nm emission (Figure 6b) should be mostly attributed to the recombination of electron and hole trapped in LUMO 1 and HOMO 1, respectively. Other donor or acceptor surface states can also be involved in the recombination process with both HOMO 1 and LUMO 1, and their mark can be seen as the short wavelength shoulder on the red peak in traces 2 and 3 in Figure 6b.

What are the consequences of the delocalized nature of the new surface states on the radiative and nonradiative processes in modified NPs? From the studies of delocalized states in metal complexes from the ruthenium bipyridine family, it is known that the delocalization reduces the electronic-to-vibration coupling constant of the transition from the delocalized state to the ground state.[56−60] Additionally, it reduces the rate of thermally activated transition to the metal-centered states.[56] Both effects decrease the rate of nonradiative processes, which results in a substantial extension of the lifetime of delocalized states, in some cases as much as 3000 times.[57,61] Recently, a similar phenomenon was reported for a series of copper bis(phenanthroline) complexes, which is directly related to the surface states of CuBM-modified CdS.[62] Note that the effect of delocalization on the lifetime of the excited states appears to be quite general and can be observed in metal complexes,[58,59,63] poly(thiophene),[64,65] and triphenylene columnar liquid crystals.[66]

(50) Wandelt, K.; Hulse, J.; Kueppers, J. *Surf. Sci.* **1981**, *104*, 212−239.
(51) Dolle, P.; Alnot, M.; Ehrhardt, J. J.; Thomy, A.; Cassuto, A. *Bull. Soc. Chim. Fr.* **1985**, 329−332.
(52) Dedecek, J.; Sobalik, Z.; Tvaruazkova, Z.; Kaucky, D.; Wichterlova, B. *J. Phys. Chem.* **1995**, *99*, 16327−16337. Moine, B.; Pedrini, C.; Boutinaud, P.; Parent, C.; Le Flem, G. *J. Lumin.* **1991**, *48−49*, 515−516. Boutinaud, P.; Parent, C.; Le Flem, G.; Pedrini, C.; Moine, B. *J. Phys.: Condens. Matter* **1992**, *4*, 3031−3042. James, A. M.; Laxman, R. K.; Fronczek, F. R.; Maverick, A. W. *Inorg. Chem.* **1998**, *37*, 3785−3791.
(53) Lakowicz, J. R.; Gryczynski, I.; Gryczynski, Z.; Murphy, C. J. *J. Phys. Chem. B* **1999**, *103*, 7613−7620.
(54) Lakowicz, J. R. *Principles Of Fluorescent Spectroscopy*; Plenum Press: New York, 1986; p 496.
(55) Chandler, R. R.; Coffer, J. L.; Atherton, S. J.; Snowden, P. T. *J. Phys. Chem.* **1992**, *96*, 2713−2717.
(56) Hammarstroem, L.; Barigelletti, F.; Flamigni, L.; Indelli, M. T.; Armaroli, N.; Calogero, G.; Guardigli, M.; Sour, A.; Collin, J. P.; Sauvage, J. P. *J. Phys. Chem. A* **1997**, *101*, 9061−9069.
(57) Grosshenny, V.; Harriman, A.; Romero, F. M.; Ziessel, R. *J. Phys. Chem.* **1996**, *100*, 17472−17484.
(58) Boyde, S.; Strouse, G. F.; Jones, W. E., Jr.; Meyer, T. J. *J. Am. Chem. Soc.* **1990**, *112*, 7395−7396.
(59) Strouse, G. F.; Schoonover, J. R.; Duesing, R.; Boyde, S.; Jones, W. E. J.; Meyer, T. J. *Inorg. Chem.* **1995**, *34*, 473−487.
(60) Li, C.; Hoffman, M. Z. *Inorg. Chem.* **1998**, *37*, 830−832.
(61) Aarnts, M. P.; Stufkens, D. J.; Wilms, M. P.; Baerends, E. J.; Vlcek, A., Jr.; Clark, I. P.; George, M. W.; Turner, J. J. *Chem.-Eur. J.* **1996**, *2*, 1556−1565.
(62) Miller, M. T.; Gantzel, P. K.; Karpishin, T. B. *Inorg. Chem.* **1999**, *38*, 3414−3422.
(63) Danielson, E.; Lumpkin, R. S.; Meyer, T. J. *J. Phys. Chem.* **1987**, *91*, 1305−1306. Humbs, W.; Strasser, J.; Yersin, H. *J. Lumin.* **1997**, *72−74*, 677−678. Humbs, W.; Yersin, H. *Inorg. Chem.* **1996**, *35*, 2220−2228. Braun, D.; Huber, P.; Wudy, J.; Schmidt, J.; Yersin, H. *J. Phys. Chem.* **1994**, *98*, 8044−8049. Yersin, H.; Braun, D. *Coord. Chem. Rev.* **1991**, *111*, 39−46. Baiano, J. A.; Murphy, W. R. *Inorg. Chem.* **1991**, *30*, 4594. Downard, A.; Steel, P. *Inorg. Chem.* **1991**, *30*, 2259.

Thus, the elongation of the emission lifetime observed for the 630−750 nm band is the natural outcome of the change of the nature of the transition responsible for the red luminescence. Instead of the transition between localized surface traps in naked CdS, the quanta are emitted now due to the transition between delocalized HOMO 1 and LUMO 1 involving the aromatic π-system of the organic ligands in the orbitals. The reason for the decrease of the overall luminescent intensity is not fully understood at this moment. Secondary photochemical processes are considered to be the likely reason for that.

Now, let us look at the sequence of the calculated energy levels. Besides the delocalized states, there exist HOMOs and LUMOs, which are quite localized. In particular, there are LUMOs preferentially centered on the metal complex side of the supramolecule, which should retain mainly the properties of the corresponding orbitals of the CuBM complex (Figure 8d,e). If the calculated ladder of energy levels in Figure 8 is correct, then the excitation into the higher LUMO states should lead to the subsequent relaxation into LUMO 1, and, after that, the recombination with hole in HOMO 1 can occur which can be seen as the corresponding emission. These processes can be probed by the excitation spectra of the prepared supramolecules. In the experiment, the excitation spectrum registered at 670 nm after the attachment of CuBM displays the characteristic double peak of the copper complex (Figure 7b, trace 2), which is somewhat shifted as compared to the UV absorption of free CuBM in water (Figures 2a, trace 1) due to the formation of the Cu−S bond (see above). This peak shows that there are indeed some LUMOs, which maintain mainly the optical properties of the CuBM complex, and the excitation of the supramolecule to these LUMOs does lead to the 630−750 nm emission. This observation experimentally substantiates the calculated sequence of LUMOs in the supramolecule. Importantly, as evidenced by the excitation spectrum (Figure 7b), the LUMO 1 → HOMO 1 emissive state can be populated from both the CdS side and the CuBM sides. This can be seen as a presence of adsorption features of both CdS (adsorption edge and a small maximum at 360 nm) and those of CuBM (double peak at 300 nm), which is the direct consequence of the delocalized nature of the frontier orbitals. Interestingly, the CuBM band is significantly stronger than the excitonic features of the NPs. This intensity increase occurs due to high efficiency of population of the emissive states via the ladder of fairly strongly CuBM-localized LUMO orbitals leading inevitably to LUMO 1. On the CdS side, the excitation of the NP core states responsible for the observed spectral features in the excitation spectrum is coupled to a fairly large number of nonradiative recombination pathways reducing the efficiency of energy transfer.

Conclusion

The technique of chalcogen modification of NP involves the reaction of the mixed ligand transition metal complex with strong bidentate ligands and weak monodentate ligands. In the course of the reaction, the weak ligand is replaced with a transition metal−chalcogen bond, and the remaining part of the complex becomes attached to the surface of CdS NP. NP with multiple (2,2′-bipyridyl-*N*,*N*′)(malonato-*O*,*O*′)-copper(II) units attached constitutes a new type of supramolecular species assembled from qualitatively different chromophores. Molecular orbital calculations and experimental data indicate that surface states delocalized over the NP atoms, transition metal, and π-system of the aromatic orbital develop as a result of the surface modification. Butterfly d-atomic orbitals of the transition metals make possible such bridging, which cannot be realized for surface modification of cadmium sites on CdS NPs. The delocalized surface states strongly affect NP photophysics by altering the carrier dynamics on the surface as demonstrated by the new luminescence features. One should also expect a strong effect of such states on charge injection into the NPs, which is of great interest for many applications of NPs.

Acknowledgment. The funding from NSF-CAREER (CHE-9876265), AFOSR (F49620-99-C-0072), OCAST, and Nomadics Inc. to N.A.K., which made this work possible, is gratefully acknowledged. Funds for the 400 and 600 MHz NMR spectrometers for the Oklahoma Statewide Shared NMR facility were provided by the National Science Foundation (Grant BIR-9512269), the Oklahoma State Reagents for Higher Education, the W. W. Keck Foundation, and Conoco Inc. J.R. gratefully acknowledges financial support from CONACYT through Project Number 25059-E and is grateful to DGSCA-UNAM for providing a supercomputer (ORIGIN 2000 series) account. The authors are grateful to Prof. Jin-Joo Song and Dr. Gordon Gainer from the Center of Laser and Photonics Research of OSU for the help with some time-resolved luminescence measurements. We also would like to thank Prof. Giersig from the Hahn-Meitner Institute (Berlin, Germany) for the transmission microscopy imaging of the nanoparticles, Prof. Penger Tong from OSU for light-scattering measurements, and the group of Prof. Weller in Hamburg for insightful discussions at the onset of this project.

Supporting Information Available: X-ray diffraction of CdS NPs, representative TEM images and particle size distribution before and after the reaction with CuBM, and the UV−vis spectra of CuBM before and after the reaction with aqueous solution of Na_2S (PDF). This material is available free of charge via the Internet at http://pubs.acs.org.

JA017149A

(64) Rumbles, G.; Samuel, I. D. W.; Magnani, L.; Murray, K. A.; DeMello, A. J.; Crystall, B.; Moratti, S. C.; Stone, B. M.; Holmes, A. B. *Synth. Met.* **1996**, *76*, 47−51.
(65) de Souza, M. M.; Rumbles, G.; Gould, I. R.; Amer, H.; Samuel, I. D. W.; Moratti, S. C.; Holmes, A. B. *Synth. Met.* **2000**, *111*−*112*, 539−543.
(66) Markovitsi, D.; Germain, A.; Millie, P.; Lecuyer, P.; Gallos, L.; Argyrakis, P.; Bengs, H.; Ringsdorf, H. *J. Phys. Chem.* **1995**, *99*, 1005−1017.
(67) Rockenberger, J.; Troger, L.; Kornowski, A.; Vossmeyer, T.; Eychmuller, A.; Feldhaus, J.; Weller, H. *Ber. Bunsen-Ges. Phys. Chem.* **1997**, *101*, 1613−1616.